Mode coupling by plasmonic surface scatterers in thin-film silicon solar cells

M. van Lare,[1] F. Lenzmann,[2] M. A. Verschuuren,[3] and A. Polman[1]
[1]*Center for Nanophotonics, FOM Institute AMOLF, Science Park 104, Amsterdam 1098 XG, The Netherlands*
[2]*Energy Research Center of The Netherlands ECN, P. O. Box 1, 1755 ZG Petten, The Netherlands*
[3]*Philips Research Laboratories, High Tech Campus 4, 5656 AE Eindhoven, The Netherlands*

(Received 18 July 2012; accepted 4 November 2012; published online 27 November 2012)

We demonstrate effective mode coupling by light scattering from periodic Ag nanoparticle arrays printed onto a completed thin-film a-Si:H solar cell. Current-voltage measurements show a photocurrent enhancement of 10% compared to a flat reference cell with a standard antireflection coating. External quantum efficiency measurements for the nanopatterned cells show clear infrared photocurrent enhancement peaks, corresponding to coupling to discrete waveguide modes in the a-Si:H layer. The data are in good agreement with three-dimensional finite element simulations, which are used to further optimize the design. We show that broadband photocurrent enhancement can be obtained over the 450–750 nm spectral range. © *2012 American Institute of Physics*.
[http://dx.doi.org/10.1063/1.4767997]

Thin-film solar cells offer the potential of high photovoltaic conversion efficiency combined with low fabrication costs and the possibility of a mechanically flexible design. The major disadvantage of thin-film cells over their thick counterparts is the relatively poor absorption of light, in particular in the infrared part of the solar spectrum. To overcome this problem, light trapping is required, in which light scattering structures are integrated within the solar cell to trap the light in multiple ways: The scattering leads to an angular redistribution of the light; in this way, the path length of a single pass is enhanced and light at angles above the critical angle, it is trapped by total internal reflection. Furthermore, parallel momentum obtained in the scattering process can be used to couple to in-plane waveguide modes.[1–3]

Metal nanoparticle arrays have been proposed as efficient light coupling and trapping coatings in thin-film solar cells. Metal nanoparticles are known to have high scattering cross sections near their plasmon resonance wavelength,[4,5] which can be tuned by varying the dielectric environment, and particle size or shape. Two main geometries have been considered. In the first, metal nanostructures are embedded in the metal back contact of the solar cell. The nanoparticle array then scatters light that is poorly absorbed in its first pass through the active layer of the cell into in-plane waveguide modes of the cell, thereby enhancing the light trapping.[6–8] In the second geometry, metal nanoparticles are placed at the front-surface of the cell. In that case, they serve a dual purpose: they enhance the coupling of light into the cell by reducing reflection from the cell (anti-reflection effect), and they can enhance the path length in the cell (light trapping).[9–13]

So far, the anti-reflection effect, which is due to the preferential forward scattering from the plasmonic resonances, has been studied in detail.[14,15] The light trapping effect for plasmonic surface coatings, however, has not been well investigated. Here, we study the application of a Ag nanoparticle array on top of a completed solar cell that includes a dielectric antireflection coating. We find that the Ag nanoparticles scatter light into distinct waveguide modes of the solar cell, clearly enhancing the infrared response of the solar cell. Near-field enhancement does not play a role here, since the particles are separated from the cell by a 80 nm indium-tin-oxide (ITO) layer. Numerical simulations show that the effect can be further enhanced. Our work is applicable to other solar cell materials and designs as well.

Thin-film hydrogenated amorphous silicon (a-Si:H) solar cells were used in this study. The fabrication of the solar cells was carried out as described by Soppe *et al.*[16] Silica glass substrates were first sputter-coated with a 200 nm Ag layer followed by 80 nm ZnO buffer layer. The a-Si:H, with an intrinsic layer thickness of 350 nm, is grown in a *n-i-p* sequence using plasma enhanced chemical vapor deposition. 4×4 mm^2 pads of 80-nm-thick ITO were then sputter-coated on top through a contact mask, to define the cell areas. The ITO serves as an antireflection coating as well. Finally, U-shaped Ag contacts are sputtered on top of the ITO, using a contact mask. The inset in Fig. 1 shows a schematic cross section of the solar cell.

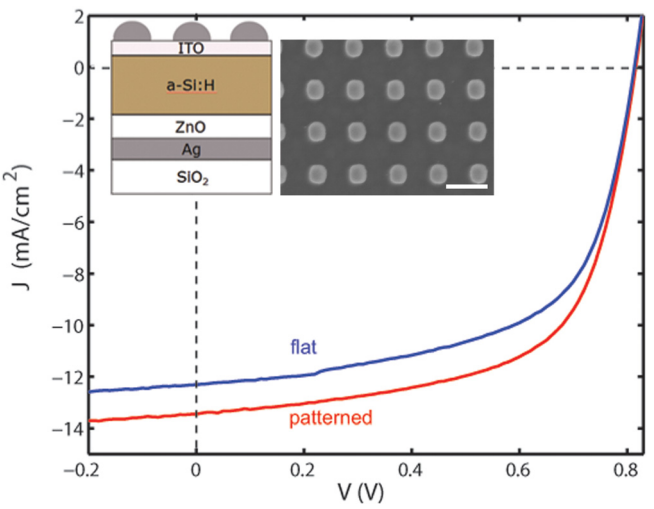

FIG. 1. *I-V* curve for a Ag nanopatterned a-Si:H solar cell (500 nm pitch, 120 nm height, and 120 nm radius, red) and a flat reference cell (blue). The insets show a schematic cross section of the layer structure and a top-view SEM image of the particle array (scale bar 500 nm).

Metal nanoparticle arrays were printed on top of the completed cell using substrate conformal imprint lithography (SCIL). This technique enables inexpensive high-fidelity nanopatterning on large-area samples and is compatible with standard solar cell manufacturing techniques. SCIL uses a bilayer rubber stamp composed of a thin high-Young's-modulus polydimethylsiloxane (PDMS) layer that holds the nanostructures, laminated to a thick low-modulus-PDMS layer that gives the stamp flexibility.[17]

In the imprint process, a layer of polymethylmethacrylate (PMMA) followed by a layer of silica-based sol-gel are spin-coated on the solar cell. Next, the rubber stamp is used to print an array of holes in the sol-gel. Anisotropic reactive ion etching (RIE) with a gas mixture of CHF_3 and Ar is then used to remove the thin residual sol-gel layer on the bottom of the holes. Subsequently, the holes are transferred into the PMMA using O_2 reactive ion etching. A 120 nm thick layer of Ag is then thermally evaporated on the sample. Finally, lift-off of the PMMA layer is performed in acetone, so that an array of Ag particles remains. The inset of Fig. 1 shows an SEM image of the particle array on the solar cell. The square array has a pitch of 500 nm, and the particles have a radius and height of 120 nm. This image shows that the metal nanoparticles can be accurately printed on top of a completed a-Si:H solar cell.

Figure 1 shows the current-voltage (*I-V*) curves for both the patterned (red) and the reference cell (blue). *I-V* curves are measured with a Wacom solar simulator under 1 sun illumination. Both cells have an open circuit voltage $V_{oc} = 810$ mV; the fill factors are also similar: $FF = 0.60$ and $FF = 0.61$ for the patterned and reference cells, respectively. This indicates that the SCIL imprint process is well compatible with solar cell manufacturing and does not lead to additional non-radiative recombination or cell shunting. The short-circuit current densities are $J_{sc} = 13.7$ mA/cm^2 and $J_{sc} = 12.5$ mA/cm^2, for the patterned and reference cells, respectively. The enhanced light coupling by the metal nanoparticle array thus leads to a 10% photocurrent enhancement. Note that this enhancement is observed beyond a reference cell that had an optimized ITO anti-reflection coating. Most other studies on metal nanoparticle enhanced light coupling do not use a cell with optimized anti-reflection coating as reference.[18–21]

Figure 2 shows external quantum efficiency (EQE) measurements of cells with (red) and without (blue) the Ag nanoparticle array. The EQE measurements were carried out on a commercial spectral response set-up by Optosolar (SR300) using a 250 W xenon lamp. Data are taken in 10 and 20 nm wavelength intervals for the patterned and reference cells, respectively. The peaks observed in the $\lambda = 600$–800 nm spectral band are highly reproducible. For the flat cell, the spectral response is a smooth function of wavelength with the exception of the peak at $\lambda = 650$ nm, which is attributed to a Fabry-Perot effect in the a-Si:H layer. In contrast, the patterned cell shows multiple peaks in the near-infrared, at $\lambda = 660$ nm, $\lambda = 690$ nm, and $\lambda = 730$ nm. These are clear signatures of coupling to the waveguide modes as will be discussed below. While the metal nanoparticle array thus clearly enhances the spectral response in the infrared, it causes a reduced response in the blue spectral range, when

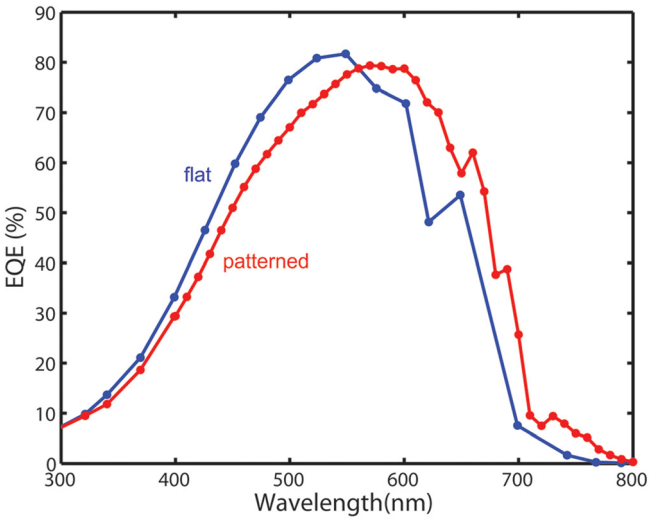

FIG. 2. External quantum efficiency spectra for the patterned (red) and flat reference cell (blue).

compared to the reference. This is attributed to Ohmic dissipation in the metal particle on resonance and increased reflection below the particle resonance. The latter is due to the Fano effect: the destructive interference between the directly transmitted beam and the forward scattered light at wavelengths below the plasmon resonance.[7,10,11,22]

Due to its high refractive index ($n = 3.9$–5.5 in the 350–800 nm spectral range), light is very well confined in the a-Si:H waveguide layer. Figure 3 shows the calculated dispersion relation for the lowest-order waveguide modes in the a-Si:H layer, taking into account all layers in the solar cell. In the wavelength range where light trapping is important ($\lambda > 550$ nm), the layer structure supports ten modes; five transverse electric (TE) and five transverse magnetic (TM) modes. The black dashed-dotted line shows the light line in air. All modes are located to the right of the light line,

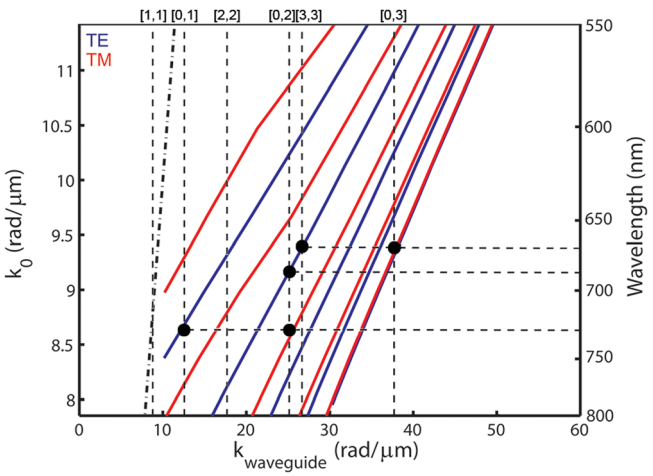

FIG. 3. Dispersion relations for the TE (blue) and TM (red) waveguide modes in the 350-nm a-Si:H layer. The black dashed-dotted line is the light line in air. The vertical black dashed lines are the grating orders provided by the experimental particle array, which has a pitch of 500 nm. At wavelengths where these lines cross the waveguide modes, light incident at normal incidence can couple to waveguide modes. The three horizontal black dashed lines show the incident wavelengths at which peaks appear in the EQE measurement of Fig. 2.

meaning that they are purely bound and cannot couple to free space radiation (light trapping). The vertical lines indicate the in-plane momentum provided by the grating orders as a result of the periodic nature of the Ag particle array. At wavelengths where the modes cross these grating lines, coupling is possible for light incident at normal incidence. The uncertainty in the modal wavevector due to absorption in the a-Si:H layer causes momentum matching to occur over a broader spectral range (not shown here).

Next, we compare the measured EQE peaks for the nanopatterned sample with the dispersion calculations. The horizontal lines in Fig. 3 reflect the experimentally observed EQE peak wavelengths for the particle array from Figure 2. Clearly, the three observed peaks each correspond to distinct intersections of the dispersion curves with the grating vectors. The peak in EQE at $\lambda = 660$ nm corresponds to the [3,3] grating order coupling to the TE_3 mode and the [0,3] grating order coupling to the TE_0 and TM_0 mode. The peak at $\lambda = 690$ corresponds to the [0,2] grating order coupling to the TE_3 mode. Finally, the peak at $\lambda = 730$ nm corresponds to the [0,2] grating-order coupling to the TM_2 mode and the [0,1] grating order coupling to the TE_4 mode. Note that not all crossings between modes and grating orders appear as clear peaks in the EQE measurement. We attribute this to the limited bandwidth of the measurement and, for shorter wavelengths, the fact that light is strongly absorbed in the a-Si:H, so that the effect of light trapping is smaller. Furthermore, coupling to higher order modes is less efficient; the higher order modes have narrower mode-profiles, leading to lower overlap between the scattered field and the field of the waveguide mode.

Three-dimensional finite difference time domain (FDTD) simulations, performed using LUMERICAL FDTD software, were used to model the absorption in the *i*-layer of the a-Si:H, taking into account the full layer structure. A unit cell with one cylindrical Ag particle is used in combination with periodic boundary conditions in x and y direction to simulate a periodic array. At the top and bottom of the simulation, volume perfectly matched layers are used. Figure 4(a) shows the fraction of incident light that is absorbed in the intrinsic a-Si:H layer as a function of wavelength (continuous lines). Simulations are shown for a flat solar cell with 80 nm ITO (blue); the experimentally studied solar cell with a 500-nm-pitch array with 120-nm-radius and 120-nm-high particles (red). The simulations reflect the experimental trends in Fig. 2 very well, with an absorption peak observed in the wavelength range $\lambda = 550$–600, corresponding to the EQE peak in Fig. 3. The coupling to waveguide modes for the patterned cell is clearly observed in the red part of the spectrum, leading to enhanced absorption in the a-Si:H layer. Peaks similar to the EQE peaks in Fig. 3 are observed in the $\lambda = 650$–750 nm spectral range. The simulation also shows reduced absorption at wavelengths below $\lambda = 600$ nm, corresponding to the reduced EQE in Fig. 3. Figure 4 shows that a purely optical model, neglecting wavelength-dependent carrier collection rates, can well predict trends in EQE.

Considering the good agreement between the FDTD simulations and the EQE measurements, we use FDTD simulations to further optimize the Ag nanoparticle array geometry. By reducing the particle diameter, the resonance, and

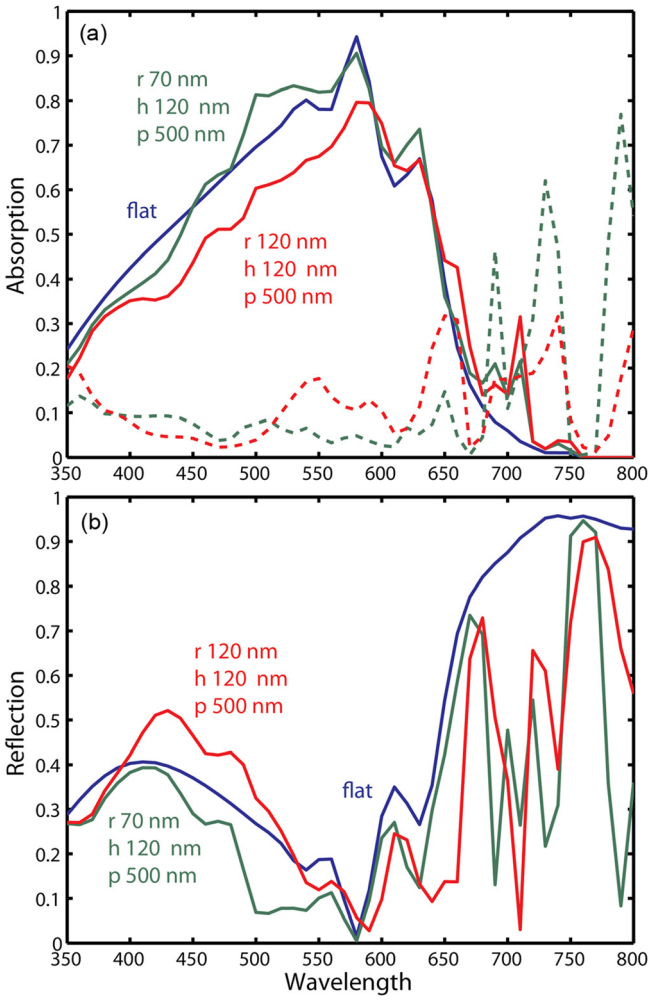

FIG. 4. (a) Simulated absorption in the a-Si:H i-layer (continuous lines) and in the Ag nanoparticles (dashed lines). (b) Simulated reflection from the layer geometry. Data are shown for the experimental nanopatterned cell geometry (red), the flat reference cell (blue), and an optimized design (green).

hence the destructive Fano interference at wavelengths below the resonance, shifts to the blue. The green continuous line in Fig. 4(a) shows the absorption spectrum for a 450-nm pitch array with 70-nm-radius and 120-nm-high Ag particles. This array shows a clearly enhanced blue response compared to the experimental array and the flat cell while maintaining a high red response. Note that the peaks in the red have shifted as a consequence of changing the array pitch (and thus the in-plane momentum provided by the grating orders). The dashed lines in Fig. 4(a) show the calculated absorption in the metal nanoparticles. As can be seen, the particle plasmon resonance, which occurs at $\lambda = 530$ nm for the experimental sample, has shifted to $\lambda = 470$ nm for the optimized array.

Finally, Fig. 4(b) shows the simulated reflectance for the flat (blue), experimental (red), and optimized (green) geometry. Using a nanoparticle array, the reflectance is clearly reduced in the (infra-)red spectral range, due to the enhanced light trapping. Indeed, clear minima in reflection are observed at wavelengths where mode coupling occurs. For the experimental sample, reflectance in the blue spectral range is higher than for the flat sample, in agreement with the Fano interference argument mentioned above. The optimized array, however, has a reflection well below that of the flat sample over

the entire spectral range from $\lambda = 350$–670 nm. In particular from $\lambda = 410$–670 nm, where the solar spectrum is intense, the reflection is well below 10%. The minima in reflection at $\lambda = 500$ and $\lambda = 450$ nm correspond to the Rayleigh anomalies for the 500 nm and 450 nm pitch geometries, respectively.

In conclusion, we fabricated a periodic array of Ag nanoparticles on top of a completed a-Si:H solar cell using substrate conformal imprint lithography. The addition of nanoparticles resulted in a 10% photocurrent enhancement with respect to the flat cell with a standard ITO antireflection coating. By comparing external quantum efficiency spectra and modal dispersion calculations, we demonstrate coupling of light scattered from the nanoparticles to distinct TE and TM waveguide modes in the a-Si:H, through second- and third-order grating coupling. The mode coupling is corroborated by three-dimensional FDTD simulations, which show that further optimization of the array geometry can simultaneously optimize the red and blue response of the cell, leading to a broadband photocurrent enhancement.

We are grateful to Jorik van de Groep for the Mathematica code used for the modesolver calculations, Maarten Dorenkamper and Klaas Bakker (ECN) for the solar cell fabrication and support with the EQE measurements. SARA Computing and Networking Services is acknowledged for support in using the Lisa Compute Cluster. This work is part of the research program of FOM, which is financially supported by NWO. It is also funded by the European Research Council, the Global Climate and Energy Project (GCEP) and NanoNextNL, a technology program of the Dutch Ministry of Economy Affairs.

[1]H. A. Atwater and A. Polman, Nature Mater. **9**, 205 (2010).
[2]E. Yablonovitch and G. D. Cody, IEEE Trans. Electron Devices **29**, 300–305 (1982).
[3]M. A. Green, Prog. Photovolt. **10**, 235 (2002).
[4]C. F. Bohren and D. R. Huffman, *Absorption and Scattering of Light by Small Particles* (Wiley, 2008).
[5]K. R. Catchpole and A. Polman, Appl. Phys. Lett. **93**, 191113 (2008).
[6]V. E. Ferry, M. A. Verschuuren, H. B. T. Li, E. Verhagen, R. J. Walters, R. E. I. Schropp, H. A. Atwater, and A. Polman, Opt. Express **18**, A237 (2010).
[7]J. Zhu, C.-M. Hsu, Z. Yu, S. Fan, and Y. Cui, Nano Lett. **10**, 1989 (2010).
[8]R. Biswas, J. Bhattacharya, B. Lewis, N. Chakravarty, and V. Dalal, Sol. Energy Mater. Sol. Cells **94**, 2337 (2010).
[9]F. J. Beck, A. Polman, and K. R. Catchpole, J. Appl. Phys **105**, 114310 (2009).
[10]Y. A. Akimov and W. S. Koh, Plasmonics **6**, 155 (2011).
[11]C. O. McPheeters, C. J. Hill, S. H. Lim, D. Derkacs, D. Z. Ting, and E. T. Yu, J. Appl. Phys **106**, 056101 (2009).
[12]R. A. Pala, J. White, E. Barnard, J. Liu, and M. L. Brongersma, Adv. Mater. **21**, 3504 (2009).
[13]C. Rockstuhl, S. Fahr, and F. Lederer, J. Appl. Phys. **104**, 123102 (2008).
[14]P. Spinelli, M. Hebbink, R. de Waele, L. Black, F. Lenzmann, and A. Polman, Nano Lett. **11**, 1760 (2011).
[15]P. Spinelli, C. van Lare, E. Verhagen, and A. Polman, Opt. Express **19**, A303 (2011).
[16]W. J. Soppe, H. Borg, B. B. van Aken, C. Devilee, M. Dörenkämper, M. Goris, M. C. R. Heijna, J. Löffler, and P. Peeters, J. Nanosci. Nanotechnol. **11**, 10604 (2011).
[17]M. A. Verschuuren, Ph.D. dissertation, Utrecht University, Utrecht, 2010.
[18]I. Diukman and M. Orenstein, Sol. Energy Mater. Sol. cells **95**, 2628 (2011).
[19]S. Pillai, K. R. Catchpole, T. Trupke, and M. A. Green, J. Appl. Phys. **101**, 093105 (2007).
[20]A. Ji, Sangita, and R. P. Sharma, J. Phys. D: Appl. Phys. **45**, 275101 (2012).
[21]A. Pors, A. V. Uskov, M. Willatzen, and I. E. Protsenko, Opt. Commun. **284**, 2226 (2011).
[22]S. H. Lim, W. Mar, P. Matheu, D. Derkacs, and E. T. Yu, J. Appl. Phys. **101**, 104309 (2007).